Magnetized relativistic accretion disk around a spinning, electrically charged, accelerating black hole: Case of the *C* metric

Shokoufe Faraji[*] and Audrey Trova[†]
Center of Applied Space Technology and Microgravity (ZARM), 28359 Germany

Vladimir Karas[‡]
Astronomical Institute, Czech Academy of Sciences, Boční II 1401, 141 00 Prague, Czech Republic

(Received 11 February 2022; accepted 21 April 2022; published 16 May 2022)

This paper examines the general relativistic model of a geometrically thick configuration of an accretion disk around an electrically charged black hole in an accelerated motion, as described by the *C*-metric family. We aim to study effects of the spacetime background on the magnetized version of the thick disk model via the sequences of figures of equilibrium. While maintaining the assumption of non-self-gravitating (test) fluid, we newly explore the influence of the strength of the large-scale magnetic field with field lines organised over the length scale of the black-hole horizon. We systematically analyze the dependence on a very broad parameter space of the adopted scenario. We demonstrate that the *C* metric can, in principle, be distinguished from Kerr black-hole metric by resolving specific (albeit rather fine) features of the torus, such as the location of its center, inner, and outer rims, and the overall shape. The analytical setup can serve as a test bed for numerical simulations.

DOI: 10.1103/PhysRevD.105.103017

I. INTRODUCTION

Black holes are the most extreme astrophysical sources of the gravitational field in our Universe: they create an event horizon, hide a singularity, accrete and eject matter from their vicinity, exhibit frame-dragging effects that act on the surrounding particles and fields, produce gravitational waves by violent collisions, etc., (see, e.g., Refs. [1–4]). An outstanding series of available observations leads to a general agreement that the properties of many astrophysical objects could be best explained in the framework of the black-hole accretion disk scenario [5,6].

One of the theoretical models of accretion disks is the picture of a geometrically thick fluid configuration tori in a stationary, axially symmetrical structure and no magnetic field. This scheme was first introduced in seminal works of the early 1970s [7–14]. This model provides a general method to build figures of equilibrium of the perfect fluid orbiting around an isolated, stationary symmetric black hole. Self-gravity of the fluid was neglected. Later, by confirming the decisive role of magnetic fields for the fluid effective viscosity [15], Komissarov proposed an analytical version of the magnetized black-hole torus [16]. The latter work imposes various assumptions, such as the constant specific angular momentum distribution and a strictly toroidal magnetic field configuration; nonetheless, it can serve as a very useful setup for numerical tests of numerical Magnetohydrodynamics (MHD) schemes [17]. There are also studies that consider different assumptions in the setup [18–21].

The above-mentioned approaches consider accretion onto a nonrotating (Schwarzschild) or rotating (Kerr) black hole in the center of the torus. In the present work, we focus on the thick disk model in the spacetime of a spinning charged accelerating black hole described by a generalized family of the *C* metric [22,23]. The *C* metric describes the spacetime of two black holes of equal mass and opposite electric charge. The two black holes undergo acceleration that is directed away at a constant rate. The origin of acceleration can be interpreted as due to a cosmic string that causes a conical singularity and pulls the black holes away from each other. Despite that the presence of singularity complicates the global interpretation, the *C* metric can be employed as a toy model to study the effects of an accelerated black hole onto surrounding test matter within a limited region. Indeed, the origin of this acceleration which is the conical singularity can be replaced, for example, by a magnetic flux tube [24].

Originally, the *C* metric belongs to a large class of exact solutions discovered by Levi-Civita [25]. By means of a series of different, rather cumbersome transformations of the Plebański-Demiański class of electrovaccuum spacetimes [26], one could obtain the spinning, charged *C* metric. Furthermore, Hong and Teo expressed the metric in a factorized version that is easier to work and can be

[*]shokoufe.faraji@zarm.uni-bremen.de
[†]audrey.trova@zarm.uni-bremen.de
[‡]vladimir.karas@asu.cas.cz

presented in Boyer-Lindquist–type coordinates [27,28]. In fact, the maximal analytical extension of the line element describes two causally disconnected black holes accelerating in the opposite directions [29].

In this paper, we investigate this background with the aim of studying the properties of magnetized tori and the morphology of the equipotential surfaces.

In this paper, we investigate the background spacetime of the C metric with the aim of studying the properties of magnetized tori and the morphology of the equipotential surfaces. There are different motivations to consider this research. First of all, this is an exact solution to Einstein's field equation, which is worth understanding for its own sake. Besides, most of the works in the astrophysics area have been done by assuming the Schwarzschild or Kerr metrics are the best description of astrophysical compact objects in the relativistic astrophysics area. Second, astrophysical observations may not all fit within the general theory of relativity by employing just to a restricted family of Kerr spacetime [30–32]. It appears entirely natural to explore departures due to small electric charge and translatory motion of an accelerated black hole.

The C metric allows for electric charge and acceleration parameters. In fact, even if astrophysical black holes are assumed to be neutralized by their environment, a tiny net equilibrium charge may remain [33,34]. Besides, considering the acceleration parameter in this setup may provide first steps to a (semi)analytical description of stellar-mass black holes that have received recoil velocity at their formations. In fact, there is a widespread agreement that the birth kicks of black holes are necessary to explain the large distances above the Galactic plane achieved by some binaries [35] and caused the black hole to accelerate within a local cosmological medium.

In this perspective, the family of the C metric could be a hypothetical candidate for objects that exist in nature. To investigate this question, the study of its fingerprint in the observational data can be a proper first step along with analytical analysis. On the other hand, it seems the only source of information that we have in the strong gravity regime is coming from its environment, like from the shadow or accretion disks, especially with the advent of horizon-scale observations of astrophysical black holes. There is a vast amount of literature on the lensing in this metric (see, e.g., Refs. [36–39]) and its radiative nature [40,41]. To our knowledge, the influence of generalized C-metric parameters on accretion disks has not yet been properly examined.

The organization of the paper is as follows: the spacetime is briefly explained in Sec. II. The relativistic magnetized tori are presented in Sec. III. The results and discussion are presented in Sec. IV, and the conclusions are summarized in Sec. V. In this paper, the geometrized units where $c = 1$, and $G = 1$, also the signature $(-+++)$ are used.

II. SPINNING CHARGED C-METRIC

The family of the C metric has accelerating nature and is considered as describing accelerating black holes [29]. The spinning charged C metric in Boyer-Lindquist–type coordinates [28] reads as

$$ds^2 = \frac{1}{\Omega^2}\left(-\frac{f}{\Sigma}\left[dt - a\sin^2\theta\frac{d\varphi}{K}\right]^2 + \frac{\Sigma}{f}dr^2 + \Sigma r^2\frac{d\theta^2}{g} + \frac{g\sin^2\theta}{\Sigma r^2}\left[adt - (r^2+a^2)\frac{d\varphi}{K}\right]^2\right), \quad (1)$$

with the metric functions

$$\Omega = 1 + \alpha r\cos\theta, \quad (2)$$

$$f(r) = (1-\alpha^2 r^2)\left(1 - \frac{2m}{r} + \frac{e^2+a^2}{r^2}\right), \quad (3)$$

$$g(\theta) = (e^2+a^2)\alpha^2\cos^2\theta + 2m\alpha\cos\theta + 1, \quad (4)$$

$$\Sigma(r,\theta) = \frac{a^2}{r^2}\cos^2\theta + 1, \quad (5)$$

$$\xi = \alpha^2(e^2+a^2) + 1, \quad (6)$$

$$K = \xi + 2m\alpha, \quad (7)$$

where $t \in (-\infty, +\infty)$, $\theta \in (0,\pi)$, $r \in (0,+\infty)$. The metric has four independent parameters: the mass m, the electric charge e, the rotation a, and the so-called acceleration parameter α.

In this metric, $r = 0$ is the curvature singularity, and there is also a conical singularity on the θ axis. In fact, the conical deficit is associated with the presence of a cosmic string. Since the deficits along both axes $\theta = 0$ and $\theta = 2\pi$ are not the same, this imbalance tension is the origin of the driven acceleration. However, the parameter K in the metric regulates the distribution of tensions along either axis and allows φ to be 2π-periodic. It is also worth mentioning that a negative deficit is also possible; however, theoretically, this would be sourced by a negative energy object.

Almost all analysis considering the family of the C metric revolves around the coordinate ranges, which are dictated by the metric functions and their root configurations. First of all, the conformal factor Ω determines the location of the boundary

$$r_b = -\frac{1}{\alpha\cos\theta}. \quad (8)$$

In addition, the roots of metric function $f(r)$ correspond to horizons. Thus, $f(r)$ should have at least one root for $r \in (0, \frac{1}{\alpha})$ to have a black hole in the spacetime. In general, mostly with nonvanishing charge e, generic configurations

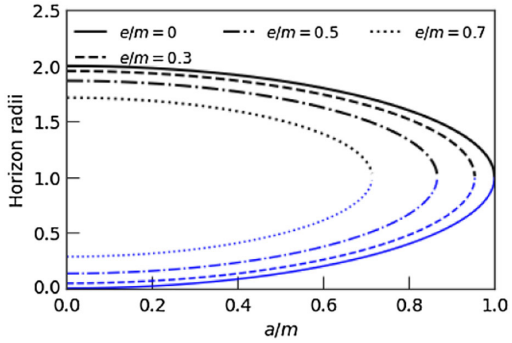

FIG. 1. Places of horizons as a function of rotation parameter a, for different charge parameter e.

have different distinct horizons. In fact, they happen to be in a pair where they are known as inner and outer horizons. Like the regular Reissner-Nordstroem solution, they typically approach one another and vanish for relatively high charge. Furthermore, when the acceleration horizon is present, there is a second outer acceleration horizon, and both intersect with the boundary. In general, the pairs of horizons separated the spacetime into different regions which share the same signature. For astrophysics point of view, we are interested in studying the accretion disk in the outer communication region between the outer horizon and the acceleration horizon. In Fig. 1, the places of the inner and outer horizons are presented for the chosen parameters. As we see, by increasing e, the places of horizons become closer to each other and to the black hole. However, since the accelerating horizon depends on α, the valid region becomes wider. The same behavior is expected for increasing a, as the metric function $f(r)$ is symmetric in parameters e and a.

Finally, from the analyzing the θ coordinate, the metric function $g(\theta)$ should have positive roots in $[0, \pi]$. Therefore, it is required to have

$$e^2 + a^2 \leq m^2, \tag{9}$$

and the following condition should be fulfilled:

$$2m\alpha \leq \begin{cases} 2\sqrt{\xi - 1} & \xi > 2, \\ \xi & 0 < \xi \leq 2. \end{cases} \tag{10}$$

Figures 2 and 3 show different parametric setups. The hatched parts are the excluded regions by Eq. (10) for chosen parameters. We see that this condition acts as an upper bound on the rotation or the acceleration for relatively small parameters. Figure 4 shows the metric function $g(\theta)$ for chosen parameters. As it has shown, the forbidden region is the hatched part, which shrinks as a and e increase since $g(\theta)$ is also symmetric with respect to a and e.

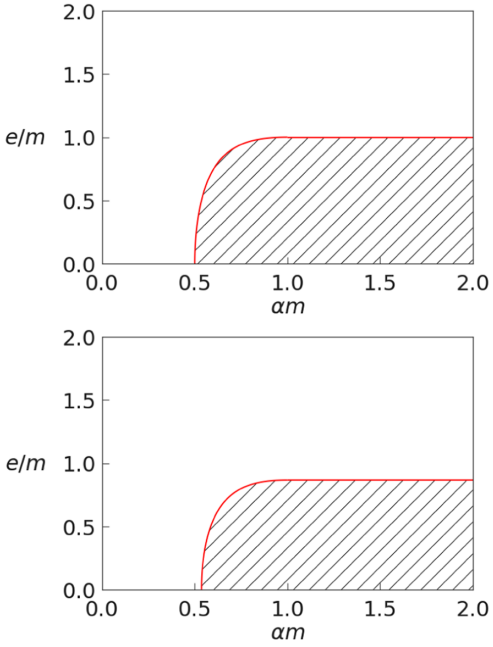

FIG. 2. Allowed parametric regions for the spinning charged C metric as a function of e. The regions marked out with hatching correspond to the forbidden regions. The first one represents the result for $a = 0$, and the second one represents the result for $a = 0.5$.

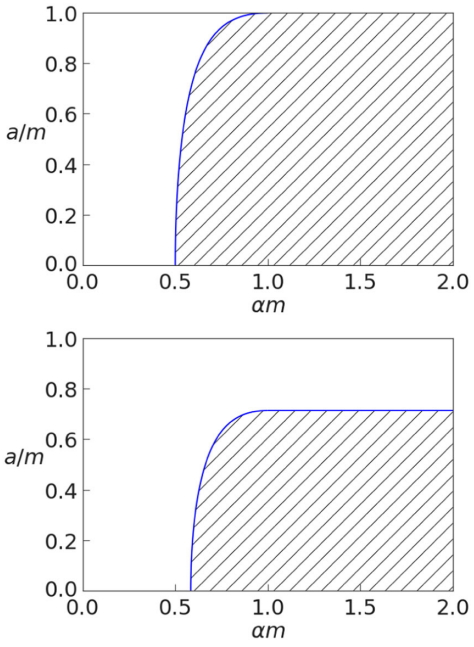

FIG. 3. Allowed parametric regions for the spinning charged C metric as a function of a. The regions marked out with hatching correspond to the forbidden regions. The first one represents the result for $e = 0$, and the second one represents the result for $e = 0.7$.

Before we describe the construction of the relativistic thick disk model, we briefly discuss the modified von Zeipel radius (or radius of gyration) as an important concept of the thick disk model [42]. This radius

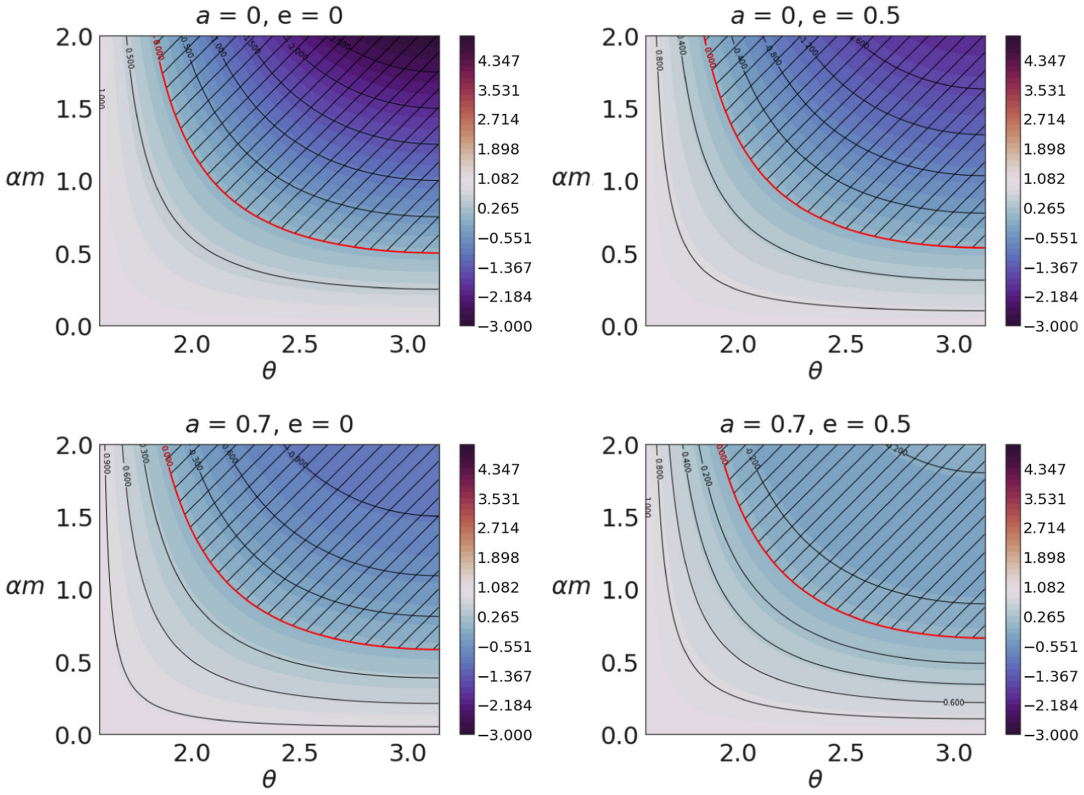

FIG. 4. Plots of metric function $g(\theta)$. The red line corresponds to $g(\theta) = 0$, and the hatched region shows $g(\theta) < 0$.

determines surfaces of constant $\mathcal{R}$, which for an axisymmetric and the stationary metric is defined as

$$\mathcal{R} = \frac{g_{\varphi\varphi}^2}{g_{t\varphi}^2 - g_{tt}g_{\varphi\varphi}}, \tag{11}$$

with respect to the stationary observers, and known as von Zeipel cylinders [43,44]. In Fig. 5, we see the effect of parameters on this radius for different sets of α, e, and a in this spacetime. In brief, this radius helps to analyze circular particles motion and provides an intuitive image of them in this spacetime; besides, this radius is related to the inertial forces. In this concept using the von Zeipel theorem, we can conclude that for a constant angular momentum distribution the surfaces of constant $\mathcal{R}$ and constant Ω coincide. This model is summarized in the next section.

III. RELATIVISTIC THICK DISK MODEL

The relativistic thick disk model considers perfect fluid equilibria of matter with the barotropic equation of state orbiting in the azimuthal direction. This equlibrium tori can study objects with sufficient radial pressure gradients, which tends to enlarge the vertical size of the disk. Additionally, it models the radiatively inefficient and non-self-gravitating accretion disks without accretion flow analytically based on Boyer's condition [45]. Within the assumption of this model, the 4-velocity and stress-energy tensor are determined by

$$u^\mu = (u^t, 0, 0, u^\varphi), \tag{12}$$

$$T^\mu{}_\nu = w u_\nu u^\mu + \delta^\mu{}_\nu p, \tag{13}$$

where the dissipation processes are neglected [46]. Here, w is the enthalpy, and p is the pressure. The relativistic Euler equation by considering the projection of conservation of stress-energy tensor into the plane normal to the 4-velocity is written as [47]

$$\int_{p_{\rm in}}^{p} \frac{\mathrm{d}p}{w} = -\ln|u_t| + \ln|(u_t)_{\rm in}| + \int_{\ell_{\rm in}}^{\ell} \frac{\Omega \mathrm{d}\ell}{1 - \Omega\ell}, \tag{14}$$

where $\ell = -\frac{u_\varphi}{u_t}$, $\Omega = \frac{u^\varphi}{u^t}$, aand the subscript *in* refers to the inner edge of the disk. The integrability condition exhibits $\Omega = \Omega(\ell)$, and this relation fulfills the relativistic von Zeipel theorem for a toroidal magnetic field [48]. This theorem states that the surfaces of constant pressure coincide with the surfaces of the constant enthalpy if and only if surfaces of constant Ω and constant ℓ coincide. In other words, the surfaces "$\mathcal{R} = $ const." coincide with the surfaces "$\Omega = $ const.," as mentioned earlier.

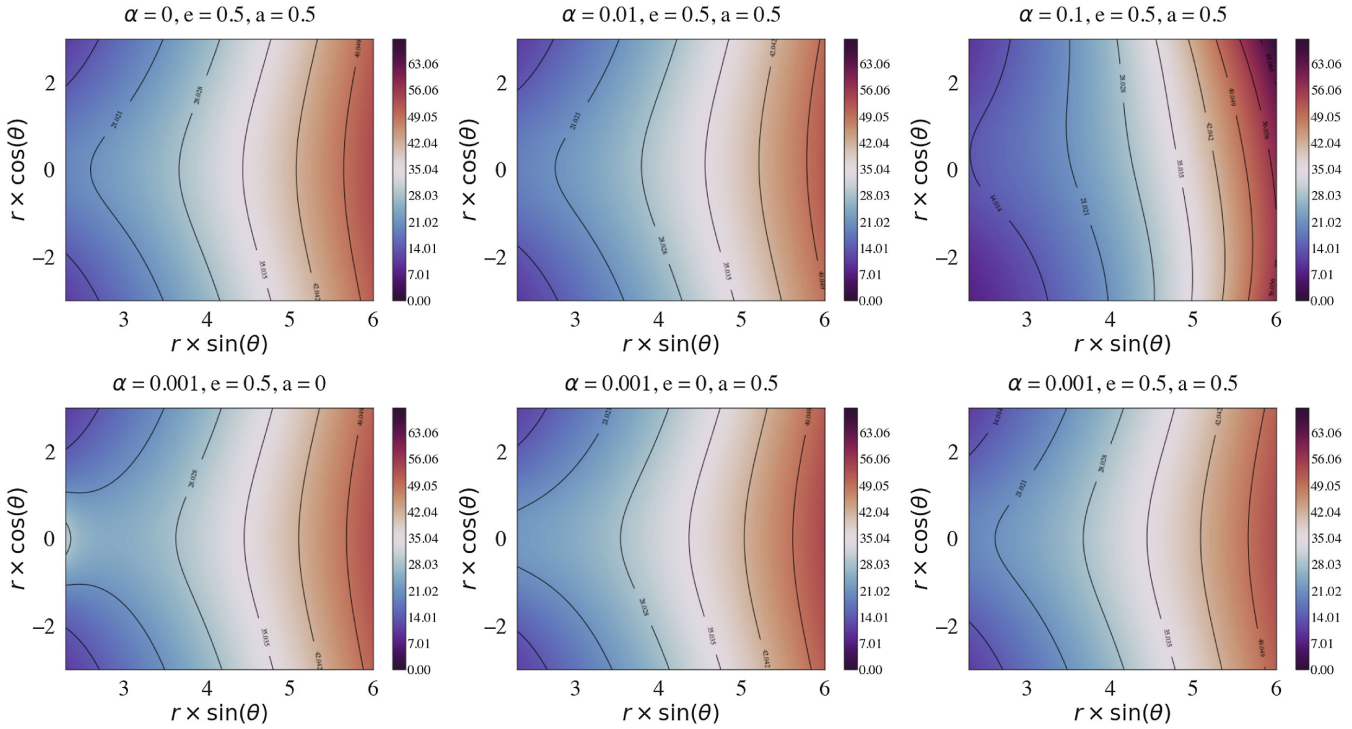

FIG. 5. Von Zeipel cylinders with respect to the stationary observers. The plots show poloidal sections across the constant $\mathcal{R}$ surfaces, where the circular timelike motion of the fluid is possible. Colors correspond to different values of the radius, as listed on the color bar to the right of each panel. Selected contours are indicated with black lines.

In what follows, we continue with the generalization of the thick disk model by considering the magnetic field that has been developed by Komissarov [16].

A. Magnetized version

The dynamical evolution of the disk model in the presence of magnetic field is governed by the following conservation laws [46,49]:

$$\nabla_\nu T^{\nu\mu} = 0, \tag{15}$$

$$\nabla_\nu(\rho u^\nu) = 0, \tag{16}$$

$$\nabla_\nu(b^\nu u^\mu - b^\mu u^\nu) = 0, \tag{17}$$

which are the energy-momentum conservation, baryon conservation, and induction equation, respectively. Here, ρ is the mass density, b^μ are the components of magnetic field and they are given by magnetic pressure in the fluid frame as $|b|^2 = 2p_{\rm m}$ [46,49]. The total energy-momentum tensor is given by

$$T^{\nu\mu} = (w + |b|^2)u^\nu u^\mu + \left(p_{\rm gas} + \frac{1}{2}|b|^2\right)g^{\nu\mu} - b^\nu b^\mu, \tag{18}$$

where $p_{\rm gas}$ is the gas pressure, and as mentioned, the dissipation processes are negligible. By assuming the model is axisymmetric and stationary,

$$u^r = u^\theta = b^r = b^\theta = 0. \tag{19}$$

Equation (14) is generalized to

$$\int_0^p \frac{{\rm d}p}{w} + \int_0^{\tilde{p}_{\rm m}} \frac{{\rm d}\tilde{p}_{\rm m}}{\tilde{w}} = -\ln|u_t| - \ln|(u_t)_{\rm in}| + \int_{\ell_{\rm in}}^{\ell} \frac{\Omega {\rm d}\ell}{1-\Omega\ell}, \tag{20}$$

where $\tilde{p}_{\rm m} = \mathcal{L}p_{\rm m}$ and $\tilde{w} = \mathcal{L}w$, with $\mathcal{L} = g_{t\varphi}^2 - g_{tt}g_{\varphi\varphi}$. To solve this equation, we assume the relations [16]

$$p = Kw^\kappa, \qquad \tilde{p}_{\rm m} = K_{\rm m}\tilde{w}^\eta, \tag{21}$$

where K, $K_{\rm m}$, κ, and η are constants. Further, $\tilde{p}_{\rm m}$ can be rewritten in terms of the magnetic pressure as $p_m = K_m\mathcal{L}^{\eta-1}w^\eta$. Equation (20) allows that on the surface of the disk and its inner edge the pressures vanish by choosing the integration constant. Thus, Eq. (20) is integrable,

$$W - W_{\rm in} + \frac{\kappa}{\kappa-1}\frac{p}{w} + \frac{\eta}{\eta-1}\frac{p_m}{w} = \int_{\ell_{\rm in}}^{\ell} \frac{\Omega {\rm d}\ell}{1-\Omega\ell}, \tag{22}$$

where $W = \ln|u_t|$. This equation implies $\Omega = \Omega(\ell)$ [47]; therefore, by choosing $\Omega = \Omega(\ell)$, equipotential surfaces W and pressure p will be determined. In addition, to fix the geometry of the equipotential surfaces, it is required to choose

angular momentum distribution ℓ. In this work, we consider the constant angular momentum ℓ_0, while choosing the constant distribution profile causes the right-hand side of Eq. (22) to vanish, and by specifying $W_{\rm in}$, one can obtain the solutions. Finally, the total potential is given by

$$W(r,\theta) = \frac{1}{2}\ln\left|\frac{\mathcal{L}}{g_{\varphi\varphi} + 2\ell_0 g_{t\varphi} + \ell_0^2 g_{tt}}\right|. \tag{23}$$

However, ℓ_0 should be chosen in the interval between the marginally stable orbit l_{ms} and the marginally bound orbit l_{mb}, to constructing a finite-size disk [47]; hence,

$$\begin{cases} W_{\rm in} \le W_{\rm cusp} & \text{if } |\ell_{ms}| < |\ell_0| < |\ell_{mb}|, \\ W_{\rm in} < 0 & \text{if } |\ell_0| \ge |\ell_{mb}|. \end{cases} \tag{24}$$

The cusp point is defined as the circle in the equatorial plane on which the pressure gradient vanishes and the specific angular momentum of the disk equals the Keplerian angular momentum. Besides, the pressure at the center of the disk, denoted by index c, is determined by

$$p_c = w_c(W_{\rm in} - W_c)\left(\frac{\kappa}{\kappa - 1} + \frac{\eta}{\beta_c(\eta - 1)}\right)^{-1}; \tag{25}$$

the center of the disk is the place where we have the maximum pressure. Here, $\beta = p/p_m$ is the magnetization parameter. The variables of the model are then u^t, u^φ, b^t, b_φ, W, w, p, and $p_{\rm m}$. Furthermore, $W_{\rm in}$ and W_c are computed from ℓ_0, and by using the equation of state one can find K and K_m, then the solution is obtained utilizing Eqs. (22) and (23).

In what follows, we present the thick disk model in this spacetime; however, because of the conical deficit, the disk does not lie on the equatorial plane, and finding conditions of existence of equipotential surfaces is a rather a challenging task.

IV. RESULTS AND DISCUSSION

In this section, we analyze the impact of the different parameters of the model on the morphology of the equipotential surfaces.

We start by examining the possibility of having solutions for this disk's model rely on the variation of the parameters. To have better insight into the role of acceleration parameter, first we consider the nonspinning case. Figure 6 shows the regions where we may have a disk in the nonspinning charged setup.

In the panel, the intersection of the dashed curve with the white and the dark-blue areas shows the possible places for choosing the center of the disk and the cusp point, respectively. As we see, the acceleration parameter α plays

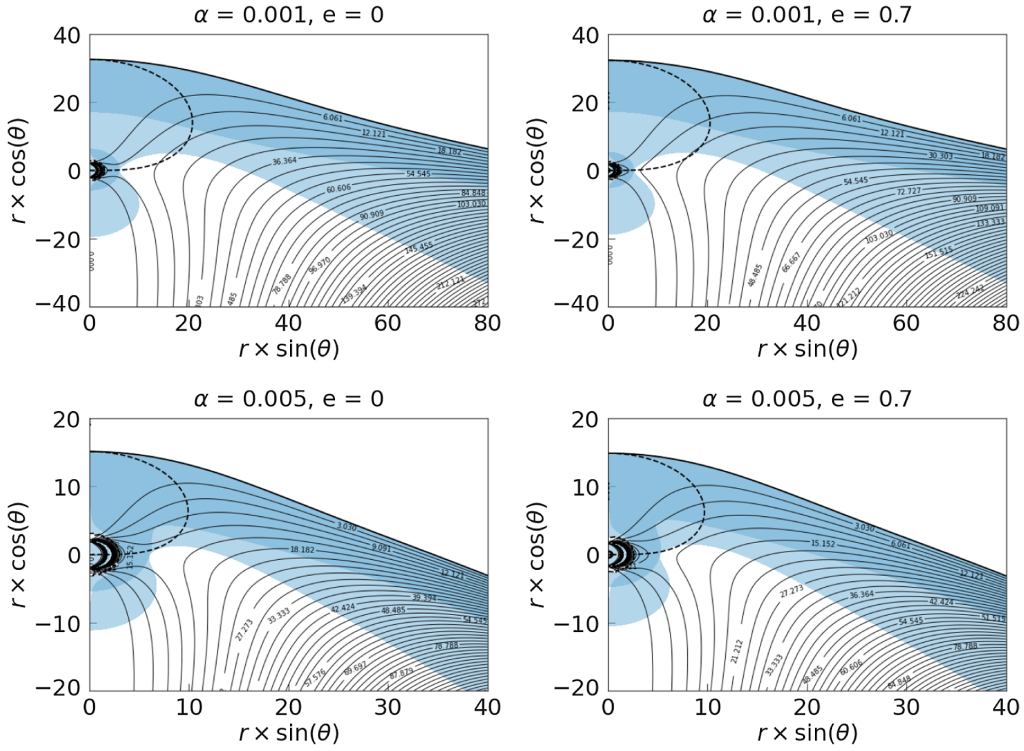

FIG. 6. Possible region for having the thick disk model. The dashed curves show when $\partial_{\rm r} W = 0$ and $\partial_\theta W = 0$. The dark blue region shows the area where the conditions for a maximum of $W(r,\theta)$ are fulfilled. The white area depicts where the conditions for a minimum of $W(r,\theta)$ are fulfilled.

a crucial role in the existence of solutions. As a result, as α even slightly increases, almost the possibility of having solutions decreases dramatically. Therefore, we can build this disk's model only for relatively small acceleration. On the other hand, the charge parameter e has an imperceptible impact and positively contributes to having solutions. Especially, the charge's effect manifests clearly when α is relatively large. For example, with a comparison in the second row for relatively large α and vanishing e, we do not have a solution, while by increasing e, we obtain solutions.

Figure 6 also shows that the distance between the center and the cusp point changes as a monotonic decreasing function of α. This leads to the larger disk structure for smaller rotation parameters a. In conclusion, as α increases with a moderate rate, the disk structure becomes smaller, and finally it vanishes. Besides, the deeper analysis of the panel manifests the possibility of the existence of two cusps for some choices of parameters.

In Fig. 7, by using Fig. 6, we choose a solution possessing an inner cusp, a center, and an outer cusp to construct the largest possible model. In Fig. 7, one can clearly see that for vanishing rotation in the first column there is the possibility of having an inner cusp and an outer cusp specified by the red curves. In addition, by increasing charge, the closed equipotential surfaces also become larger, as predicted by Fig. 6.

In columns 2 and 3 of Fig. 7, we also consider the rotation parameter a for comparison. In general, the deepest analysis reveals that the effect of the rotation parameter a on having solutions is not strong compared to α as we see in Fig. 6 but is stronger than the effect of the charge parameter e. In fact, parameter a, like α, has a negative effect on having solutions, and for relatively higher acceleration and rotation parameters, we do not find any disk structure, unless we add a relatively high charge as far as it is possible.

In Fig. 6, we see the distance between the center, and the cusp point is a monotonic increasing function of e, while it is a monotonic decreasing function of a. Therefore, the larger disk structure for bigger charge values e and smaller rotation parameters a is predicted. In other words, contrary to e, by increasing a and α, the center and the cusp's locations approach one another, and gradually we lose solutions.

Furthermore, in the second and third columns of Fig. 7 by considering rotation, the possibility of having the inner

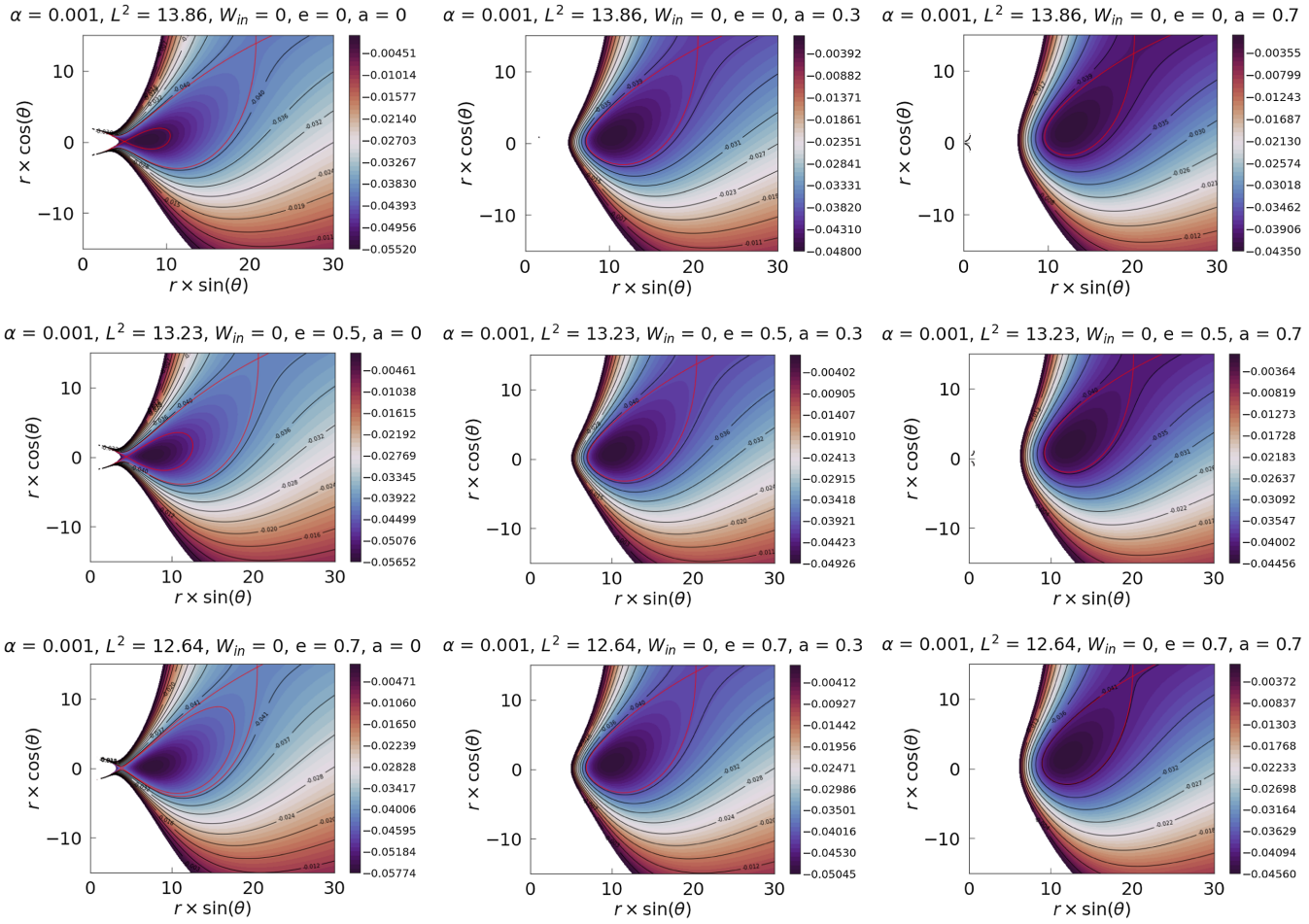

FIG. 7. Contour map of the equipotential surfaces. The red lines show the equipotential corresponding to the inner and outer cusps.

cusp is strongly reduced, while increasing the possibility of the outer cusp, in fact, leads matter to flow outward.

In addition, by increasing α and e, we obtain closed equipotential surfaces more oriented away from the horizontal axis. Of course, the effect of α is more decisive than e in this behavior; namely, as α even slightly increases, the disk deviates from the horizontal axis noticeably, which can be seen more clearly in Figs. 8 and 9.

In general, as e increases, we expect the matter to be concentrated closer to the inner edge of the disk since the slope to reach the cusp is steeper. On the contrary, the higher values of α and a more spread the matter through the disk because the value of the equipotential surface at the center and at the cusp becomes closer as a increases.

In Fig. 8, we examine the effect of the magnetization parameter β_c and the dependency of the disk structure and its orientation on the parameter e in the vicinity of the compact object for a fixed value of acceleration parameter α and vanishing rotation. In the first column we chose high magnetized model, and in the second row, we chose a relatively high charged one. In fact, comparing columns shows that the magnetization parameter does not influence the disk's geometry; however, it changes the distribution of matter inside the disk and shifts the location of the rest-mass density maximum, which is pointed out as the dashed lines in Fig. 8. In addition, comparing rows shows that we have a larger oriented disk for larger values of e. Moreover, the matter is more concentrated in the inner part of the disk, as was predicted in the previous Figs. 6 and 7.

In Figs. 9 and 10, we focus more on the impact of only one parameter α and a on the disk structure, respectively. Figure 9 presents the profound impact of α on the geometry and orientation of the disk for a fixed value of e and the magnetization parameter for the vanishing rotation. In fact, according to the last row of Fig. 6, the possibility of having solutions for relatively larger values of α depends on having large values for e, so the effect of higher α on the disk could be neutralized only partially with the higher charge values.

Figure 10 shows the dependency of the disk structure on the parameter a for the fixed parameters α, e, and β_c. As expected, increasing a changes the disk size and the distribution of matter inside the disk. Furthermore, we do not have an inner cusp for any value of rotation parameters. In addition, increasing α and a shifts the disk farther away from the compact object, contrary to an increase in e.

As a final point, it is worth mentioning that, because of the asymmetry with respect to the equatorial plane, the accretion disks in this spacetime, in general, are likely to be unstable even to axis-symmetric instabilities, which is the subject of the following work.

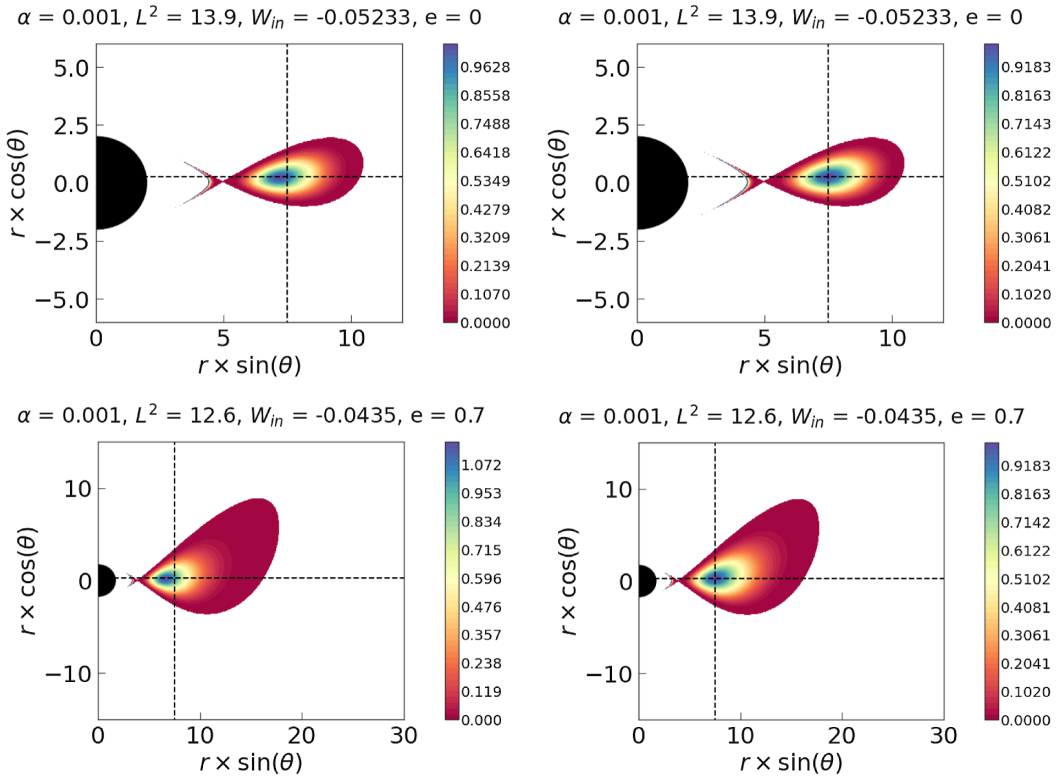

FIG. 8. Contour map of the rest-mass density of magnetized disk. The dashed lines point the center of the disk located at $r_c = 7.5$. Column 1 shows highly magnetized disk, and column 2 depicts the low-magnetized one.

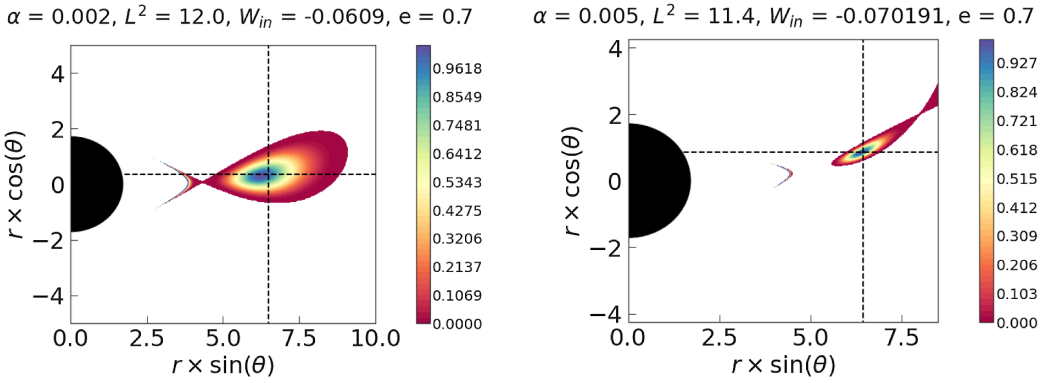

FIG. 9. Contour map of the rest-mass density of highly magnetized disc. The dashed lines point the center of the disk located at $r_c = 6.5$.

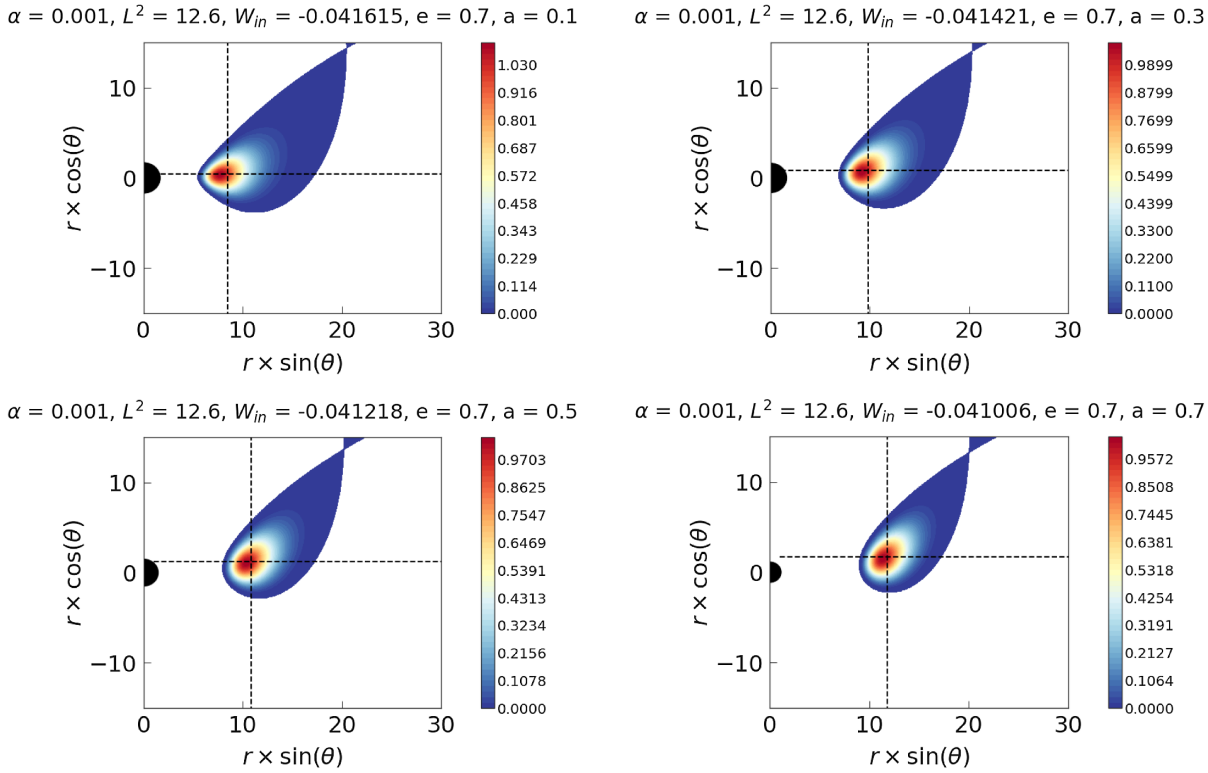

FIG. 10. Contour map of the rest-mass density of highly magnetized disk for various spin values. The dashed lines point the center of the disk. Those solutions have the same parameters (α, L, and e) of the nonrotating solution given at the bottom left of the Fig. 8.

V. CONCLUSION

In this paper, we analyzed equilibrium sequences of magnetized, non-self-gravitating disks around a spinning charged accelerating black hole. This solution is described via the generalized C-metric family, which is briefly explained in Sec. II. In this procedure, we considered the approach of Komissarov [16] to attach a dynamically toroidal magnetic field to the model.

More precisely, we have analyzed the influence of the magnetization parameter β_c, charge e, rotation a, and in particular accelerating parameter α on the structure of the magnetized thick disk model. On one hand, we have shown that changing the magnetization parameter β_c has a noticeable effect on the location and amplitude of the rest-mass density maximum, also distributing the matter inside the disk. The effect of the magnetization parameter is in complete agreement with previous studies using this model e.g., [16]. Furthermore, in this case, the range of isodensity contours increases, which is compatible with the increase of rest-mass density in the inner part of the disk.

Indeed, this result remains valid for any chosen value of other parameters.

On the other hand, we have seen the effect of varying the metric parameters: acceleration α, charge e, and rotation a on the disk's geometry, orientation, and its overall shape. We have also shown that the acceleration parameter plays a crucial role in the existence and behavior of the solutions in this setup. In conclusion, we can have the thick disk solution only for relatively small values of α, and by increasing α, the disk structure becomes smaller and slowly oriented away from the horizontal axis and gradually vanishes. Furthermore, higher values of α shift the disk farther away from the black hole. Additionally, a has a similar effect but weaker on the structure; by increasing a, the disk becomes thinner and smaller and more oriented concerning the horizontal axis until it vanishes completely. Contrary to these two parameters, an increase in e increases the disk size and the possibility of having solutions.

In addition, we have seen that e changes the distribution of matter inside the disk in the opposite way of α and a. Besides, increasing α and a shifts the disk farther from the compact object, contrary to an increase in e. However, we should *emphasize* that the strength of the parameters are not the same; among these three parameters, α has a more substantial and e has the weaker effect on the disk structure, in comparison. In general, the impact of the charge parameter is the inverse of α and a in any aspects regarding the disk properties.

As a further step of this work, the timelike circular motion can be studied. The instability of the resulting solution also deserves a proper analysis. It is also of some interest to apply these models as the initial conditions in the numerical simulations and test their ability to account for observable constraints of astrophysical systems.

ACKNOWLEDGMENTS

S. F. and A. T. thank Torben Frost for a useful discussion. S. F. thanks the Cluster of Excellence EXC-2123 Quantum Frontiers Grant No. 390837967 by the German Research Foundation (DFG). A. T. thanks the research training group GRK 1620 "Models of Gravity," funded by the German Research Foundation (DFG). V. K. acknowledges the Czech Science Foundation (Grant No. 21-11268S).

[1] C. Dewitt and B. S. Dewitt, *Black Holes. Lectures Delivered at the Summer School of Theoretical Physics of the University of Grenoble at Les Houches* (University of Grenoble, Les Houches, 1973).
[2] S. W. Hawking and W. Israel, *Three Hundred Years of Gravitation* (Cambridge University Press, Cambridge, England, 1989).
[3] Jean-Pierre Luminet, Black holes: A general introduction, in *Black Holes: Theory and Observation*, edited by Friedrich W. Hehl, Claus Kiefer, and Ralph J. K. Metzler, Lecture Notes in Physics (Springer-Verlag, Berlin, 1998), Vol. 514, pp. 3–36.
[4] Gustavo E. Romero and Gabriela S. Vila, *Introduction to Black Hole Astrophysics* (Springer-Verlag, Berlin Heidelberg, 2014), Vol. 876.
[5] Juhan Frank, Andrew King, and Derek J. Raine, *Accretion Power in Astrophysics: Third Edition* (Cambridge University Press, Cambridge, England, 2002).
[6] S. Kato, J. Fukue, and S. Mineshige, *Black-Hole Accretion Disks—Towards a New Paradigm* (Kyoto University Press, Kyoto, 2008).
[7] M. A. Abramowicz, Theory of level surfaces inside relativistic: Rotating stars. II., Acta Astron. **24**, 45 (1974).
[8] M. Kozlowski, M. Jaroszynski, and M. A. Abramowicz, The analytic theory of fluid disks orbiting the Kerr black hole, Astron. Astrophys. **63**, 209 (1978).
[9] M. Jaroszynski, M. A. Abramowicz, and B. Paczynski, Supercritical accretion disks around black holes, Acta Astron. **30**, 1 (1980).
[10] B. Paczyński and P. J. Wiita, Thick accretion disks and supercritical luminosities, Astron. Astrophys. **500**, 203 (1980).
[11] M. A. Abramowicz, M. Calvani, and L. Nobili, Thick accretion disks with super-Eddington luminosities, Astrophys. J. **242**, 772 (1980).
[12] M. A. Abramowicz, Innermost parts of accretion disks are thermally and secularly stable, Nature (London) **294**, 235 (1981).
[13] B. Paczynski, Thick accretion disks around black holes (Karl-Schwarzschild-Vorlesung 1981), Mitt. Astron. Ges. Hamburg **57** (1982).
[14] B. Paczynski and M. A. Abramowicz, A model of a thick disk with equatorial accretion, Astrophys. J. **253**, 897 (1982).
[15] Steven A. Balbus and John F. Hawley, A powerful local shear instability in weakly magnetized disks. I. Linear analysis, Astrophys. J. **376**, 214 (1991).
[16] S. S. Komissarov, Magnetized tori around Kerr black holes: Analytic solutions with a toroidal magnetic field, Mon. Not. R. Astron. Soc. **368**, 993 (2006).
[17] P. Chris Fragile and Aleksander Sadowski, On the decay of strong magnetization in global disc simulations with toroidal fields, Mon. Not. R. Astron. Soc. **467**, 1838 (2017).
[18] Sergio Gimeno-Soler and José A. Font, Magnetised polish doughnuts revisited, Astron. Astrophys. **607**, A68 (2017).
[19] Patryk Mach, Sergio Gimeno-Soler, José A. Font, Andrzej Odrzywołek, and Michał Piróg, Self-gravitating magnetized tori around black holes in general relativity, Phys. Rev. D **99**, 104063 (2019).

[20] Wojciech Dyba, Patryk Mach, and Mikołaj Pietrzyński, Toroidal magnetic fields in self-gravitating disks around black holes, Phys. Rev. D **104**, 044058 (2021).
[21] Sayantani Lahiri, Sergio Gimeno-Soler, José A. Font, and Alejandro Mus Mejías, Stationary models of magnetized viscous tori around a Schwarzschild black hole, Phys. Rev. D **103**, 044034 (2021).
[22] W. B. Bonnor, The sources of the vacuumC-metric, Gen. Relativ. Gravit. **15**, 535 (1983).
[23] Hans Stephani, Dietrich Kramer, Malcolm MacCallum, Cornelius Hoenselaers, and Eduard Herlt, *Exact Solutions of Einstein's Field Equations* (Cambridge University Press, Cambridge, England, 2009).
[24] Fay Dowker, Jerome P. Gauntlett, David A. Kastor, and Jennie Traschen, Pair creation of dilaton black holes, Phys. Rev. D **49**, 2909 (1994).
[25] T. Levi-Civita, La teoria di Einstein e il principio di fermat, Il Nuovo Cimento **16**, 105 (1918).
[26] J. F. Plebanski and M. Demianski, Rotating, charged, and uniformly accelerating mass in general relativity, Ann. Phys. (N.Y.) **98**, 98 (1976).
[27] Kenneth Hong and Edward Teo, A new form of the C-metric, Classical Quantum Gravity **20**, 3269 (2003).
[28] Kenneth Hong and Edward Teo, A new form of the rotating C-metric, Classical Quantum Gravity **22**, 109 (2005).
[29] William Kinnersley and Martin Walker, Uniformly accelerating charged mass in general relativity, Phys. Rev. D **2**, 1359 (1970).
[30] José P. S. Lemos and Oleg B. Zaslavskii, Black hole mimickers: Regular versus singular behavior, Phys. Rev. D **78**, 024040 (2008).
[31] Rajibul Shaikh, Prashant Kocherlakota, Ramesh Narayan, and Pankaj S. Joshi, Shadows of spherically symmetric black holes and naked singularities, Mon. Not. R. Astron. Soc. **482**, 52 (2019).
[32] M. A. Abramowicz, W. Kluźniak, and J. P. Lasota, No observational proof of the black-hole event-horizon, Astron. Astrophys. **396**, L31 (2002).
[33] Robert M. Wald, Black hole in a uniform magnetic field, Phys. Rev. D **10**, 1680 (1974).
[34] Michal Zajaček, Arman Tursunov, Andreas Eckart, and Silke Britzen, On the charge of the Galactic centre black hole, Mon. Not. R. Astron. Soc. **480**, 4408 (2018).
[35] Serena Repetto, Melvyn B. Davies, and Steinn Sigurdsson, Investigating stellar-mass black hole kicks, Mon. Not. R. Astron. Soc. **425**, 2799 (2012).
[36] Arne Grenzebach, Volker Perlick, and Claus Lämmerzahl, Photon regions and shadows of accelerated black holes, Int. J. Mod. Phys. D **24**, 1542024 (2015).
[37] G. W. Gibbons and C. M. Warnick, Aspherical photon and anti-photon surfaces, Phys. Lett. B **763**, 169 (2016).
[38] M. Alrais Alawadi, D. Batic, and M. Nowakowski, Light bending in a two black hole metric, Classical Quantum Gravity **38**, 045003 (2021).
[39] Torben C. Frost and Volker Perlick, Lightlike geodesics and gravitational lensing in the spacetime of an accelerating black hole, Classical Quantum Gravity **38**, 085016 (2021).
[40] J. Bičák and V. Pravda, Spinning C metric: Radiative spacetime with accelerating, rotating black holes, Phys. Rev. D **60**, 044004 (1999).
[41] Jiří Podolský, Marcello Ortaggio, and Pavel Krtouš, Radiation from accelerated black holes in an anti de Sitter universe, Phys. Rev. D **68**, 124004 (2003).
[42] H. von Zeipel, The radiative equilibrium of a rotating system of gaseous masses, Mon. Not. R. Astron. Soc. **84**, 665 (1924).
[43] M. A. Abramowicz, J. C. Miller, and Z. Stuchlík, Concept of radius of gyration in general relativity, Phys. Rev. D **47**, 1440 (1993).
[44] Sandip K. Chakrabarti, Von Zeipel surfaces. II—A catalogue, Mon. Not. R. Astron. Soc. **250**, 7 (1991).
[45] Boyer's condition states the boundary of any stationary and barotropic perfect fluid body is an equipotential surface.
[46] Angelo Marcello Anile, *Relativistic Fluids and Magneto-Fluids: With Applications in Astrophysics and Plasma Physics* (Oxford University Press, New York, 1989).
[47] M. Abramowicz, M. Jaroszynski, and M. Sikora, Relativistic, accreting disks, Astron. Astrophys. **63**, 221 (1978).
[48] O. Zanotti and D. Pugliese, Von Zeipel's theorem for a magnetized circular flow around a compact object, Gen. Relativ. Gravit. **47**, 44 (2015).
[49] W. G. Dixon, *Special Relativity: The Foundation of Macroscopic Physics* (Oxford University Press, New York, 1978).